weight 231.760. The resulting measured heat capacities are reported in Table I and shown in Fig. 1.

Discussion and Conclusions

It is apparent at once from Fig. 1 that this macrocrystalline annealed silver oxide shows no thermal anomaly at all. This disappearance of the anomalously high heat capacity from the region 20 to 45°K. is the principal result of the present investigation. The two series of measurements agree well with one another and confirm this conclusion.

Measurements below 14°K. on this sample and at various temperatures on another sample will be reported in a subsequent paper. Entropy calculations and further interpretation will be based on all of these data.

Acknowledgments.—The aid of a National Science Foundation fellowship (to R.E.G., 1953–1956) and the support of the Atomic Energy Commission are gratefully acknowledged. We thank Dr. J. K. Koehler and Dr. J. B. Ott for help in the experimental measurements and Professor W. F. Giauque for many valuable discussions.

[CONTRIBUTION FROM THE DEPARTMENT OF CHEMISTRY AND LAWRENCE RADIATION LABORATORY, UNIVERSITY OF CALIFORNIA, BERKELEY, CALIFORNIA]

Silver Oxide: The Heat Capacity from 2 to 80°K. and the Entropy; the Effects of Particle Size

BY L. V. GREGOR[1] AND KENNETH S. PITZER[2]

RECEIVED DECEMBER 30, 1961

The heat capacity of Ag_2O has been measured from 2.2 to 80°K. for a finely divided annealed sample and from 3.3 to 24°K. for a macrocrystalline annealed sample. The anomalously high heat capacity originally observed in unannealed Ag_2O between 20 and 50°K. is also found in the finely divided sample, though the anomalous region is smaller and narrower, and its maximum occurs at a lower temperature. No anomalous peak in the heat capacity of macrocrystalline Ag_2O is observed down to 3.3°K., but the heat capacity of this material is higher below 14°K. than that of the finely divided sample. The heat capacity of the various samples of Ag_2O is discussed in terms of its unusual crystal structure, and a mechanism proposed to correlate the anomalous behavior of Ag_2O below 15°K. and between 20 and 40°K. The mechanism involves the interaction of the two independent sublattices of the structure of Ag_2O, and it is proposed that for very small particles, there is a transition from a symmetric high-temperature structure to a slightly distorted low-temperature structure in the vicinity of 20 to 30°K. Revised values of the thermodynamic properties of macrocrystalline Ag_2O at 298.15°K. are given, based on the observed heat capacity data below 15°K. The results are

$$S_{298.15}^0 = 28.91 \pm 0.07 \text{ cal. deg.}^{-1} \text{ mole}^{-1}$$

$$H_{298.15}^0 - H_0^0 = 3387 \pm 5 \text{ cal. mole}^{-1}$$

$$\left(-\frac{F^0 - H_0^0}{T}\right)_{298.15} = 17.55 \pm 0.07 \text{ cal. deg.}^{-1} \text{ mole}^{-1}$$

Introduction

The preceding paper[3] together with this one describes a series of low temperature calorimetric studies undertaken with the aim of understanding the anomalously high heat capacity of Ag_2O observed by Pitzer and Smith[4] in the region 20–45°K. A second region of anomalous behavior in silver oxide was noted by Kobayashi[5] in which heat is evolved in the region 100–200° the first time that freshly precipitated and dried Ag_2O is heated through this range. Since the Pitzer and Smith measurements were made on precipitated Ag_2O which had not been annealed by heating through the 100–200° range, it seemed desirable to study more highly annealed samples.

In the first investigation, which is reported in the preceding paper, macrocrystalline Ag_2O was prepared by extended culturing of precipitated material under 200 atm. of oxygen in contact with water at 325°. It was found that the heat capacity curve was quite normal through the 15–45°K. range; in other words the anomaly had disappeared. However, the quantitative trend of heat capacity with temperature from 15 to 20°K. deviated appreciably from the Debye function. Hence it seemed wise to study this macrocrystalline material below 15°K. as well as to prepare and measure samples with characteristics intermediate between the macrocrystalline sample and the freshly precipitated and dried material.

A sample of Ag_2O was annealed without greatly changing its particle size distribution, and its heat capacity was measured from 2 to 80°K. The heat capacity of the macrocrystalline Ag_2O was also measured below 15°K. In addition, subsidiary experiments were performed to determine the surface areas of the various Ag_2O samples. Measurements of the effects of annealing on the behavior of the Ag–Ag_2O electrode are reported in another paper.[6]

Experimental Methods

Preparation of Annealed Small-particle Ag_2O.—The calorimetric sample of small-particle Ag_2O was prepared by the reaction of aqueous $AgNO_3$ with carbonate free aqueous NaOH. Only freshly boiled distilled water was used for solution preparation, washing, rinsing, etc., and all glassware and equipment were thoroughly cleaned and

(1) I.B.M. Research Center, Yorktown Heights, N. Y.

(2) Rice University, Houston, Texas.

(3) R. E. Gerkin and K. S. Pitzer, *J. Am. Chem. Soc.*, **84**, 2662 (1962).

(4) K. S. Pitzer and W. V. Smith, *ibid.*, **59**, 2633 (1937); see also H. L. Johnston and J. H. Hu, *ibid.*, **73**, 4550 (1951).

(5) K. Kobayashi, *Sci. Repts. Tohoku Univ.*, First Series, **35**, 173 (1951).

(6) L. V. Gregor and K. S. Pitzer, *J. Am. Chem. Soc.*, **84**, 2671 (1962).

treated with an oxidizing agent such as concentrated HNO_3 or acid dichromate cleaning solution. The precipitate was filtered by suction on a fritted-glass filter funnel and washed five times with boiling H_2O. The large number of washings served to remove any Ag_2CO_3, since it is more soluble than Ag_2O in hot water. The final wash water was tested with indicators to ascertain the absence of Cl^- and $CO_3^=$ and establish the pH at its proper value of ~9. The sample was dried in a stream of CO_2-free oxygen.

The dried Ag_2O was a moderately free-running dark brown powder. After samples were extracted for analysis, the Ag_2O was stored in a wide-mouth, glass-stoppered bottle in a large desiccator kept in the dark. Altogether the three separate preparations gave a total yield of about 800 g. of Ag_2O.

This precipitated silver oxide was annealed by heating 45 hr. at 180° under at least 120 atm. pressure of oxygen. The sample was contained in a covered platinum test tube within a pressure bomb. The top third of each annealing sample was discarded because a few small specks of metallic silver were noted in the top layer. Presumably this reduction to metallic silver was caused by organic dust.

Analysis yielded the theoretical composition within analytical error and the only significant impurity found was a trace of copper.

The macrocrystalline silver oxide prepared by Gerkin and Pitzer[3] was employed in additional experiments in this research. It was checked for carbonate content with the result 0.012% C. After the completion of all measurements on the samples, large batches were dissolved in perchloric acid, and small but significant residues (0.3%) were observed which dissolved in concentrated nitric acid. Presumably some reduction to metallic silver occurred in the course of loading and unloading calorimeters, etc.

Surface Area of Ag_2O.—The surface areas of various samples of Ag_2O were measured by means of the BET method,[7] using N_2 as the adsorbent gas at 77°K. The apparatus and procedure are described elsewhere.[8] In all, four samples of Ag_2O were studied:

a. macrocrystalline, annealed at 325°
b. small-particle, annealed at 180°
c. small-particle, dried at 100°
d. small-particle, dried at 25°

The results are given in Table I. Also given is the average particle size for each sample, estimated from the surface area by assuming that the samples consisted of uniform cubic particles. The surface areas of the finely divided samples are surprisingly low, since it was expected that particles of the order of ~ 300 Å. would account for a sizeable fraction of finely divided Ag_2O. Optical investigations of Ag_2O have shown that there is considerable agglomeration of the smaller particles,[9] and this may be partially responsible for the low observed surface area. Recently, Allen[10] has investigated the areas of Ag_2O powders dried at 25 and 100°. His results, using the BET method, show that the surface area varies from 0.5 to 3.0 m.²/g., averaging about 1.5 m.²/g. This is in good agreement with the data observed in this research.

TABLE I

SURFACE AREA OF Ag_2O

Sample	Surface area (meters²/g.)	Average particle dimension (mm.)
a	0.074 ± 0.01	2×10^{-2}
b	0.60 ± .1	7×10^{-4}
c	1.25 ± .05	5×10^{-4}
d	1.25 ± .05	5×10^{-4}

The results show that drying temperatures up to 100° have no apparent effect on the surface area and that annealing above the Kobayashi temperature reduces the area by about 50%. This is in accordance with the view that the annealing effect observed by Kobayashi is associated with the relief of high-energy strains and dislocations and some reduction of the surface of Ag_2O.

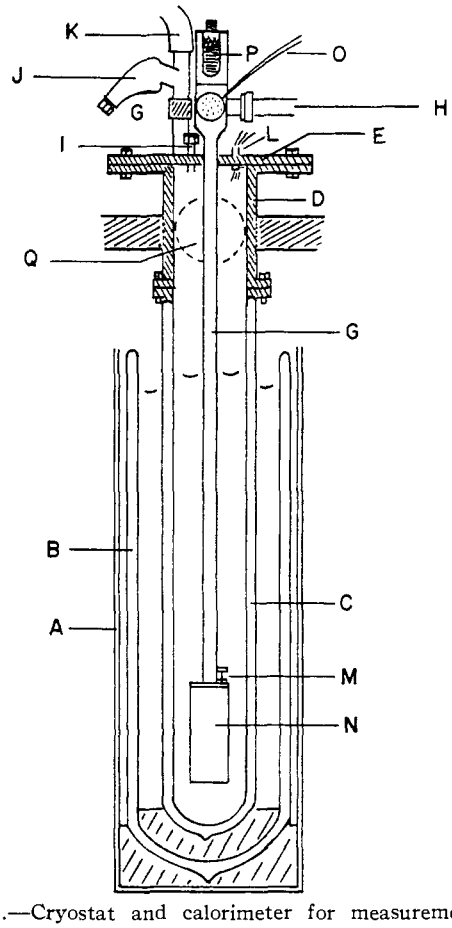

Fig. 1.—Cryostat and calorimeter for measurements at liquid-helium temperatures.

Measurement of Heat Capacities from 15 to 80°K.—Heat-capacity of annealed finely divided Ag_2O was first measured by using the procedure as well as the gold calorimeter and cryostat described by Gerkin and Pitzer.[3,9] The only difference was the use of a different platinum strain-free thermometer (Leeds and Northrup No. 1321684) as the temperature standard. (The thermometer used by Gerkin and Pitzer had been damaged.) This new thermometer had been calibrated in the laboratory from 12.25 to 335°K. at approximately 5° intervals by comparison with three similar thermometers calibrated by the National Bureau of Standards.

The total weight of Ag_2O in the calorimeter was 127.436 ± 0.003 g. *in vacuo*, or 0.5499 mole. Thermal equilibrium within the calorimeter and sample was achieved by introducing 1 atm. of helium gas into the full calorimeter before sealing it with soft solder. Care was taken not to add or subtract solder during the sealing process, and the weight of the calorimeter plus sample before and after sealing did not change within the precision of weighing for the balance used (±0.003 g.).

Apparatus for Heat Capacity Measurement from 2 to 27°K.—The heat-capacity measurements in this temperature region were made in a cryostat designed to contain liquid helium. The calorimeter was a cylinder made of copper and the thermometer was a 56-ohm, 1/2 w. carbon radio resistor. Figure 1 is a sectional sketch of the cryostat. The outer dewar (B) held liquid nitrogen and rested upon balsa supports at the bottom of the steel container (A). The inner dewar (C), which held liquid hydrogen or helium, rested upon balsa supports and was connected to a brass fitting (D). This fitting was held rigidly in place by heavy brass bars; its upper end was a flange containing an O-ring seal. A matching flange (E) was soldered to the stainless steel tube (G) (wall thickness 0.75 mm.). The tube supported the calorimeter inside its vacuum can

(7) S. Brunauer, P. H. Emmett and E. Teller, *J. Am. Chem. Soc.*, **60**, 309 (1938).

(8) T. E. Hopkins and W. F. Giauque, *ibid.*, **82**, 2426 (1960).

(9) Roger E. Gerkin, Ph.D. Dissertation, University of California, 1960.

(10) J. A. Allen, *Australian J. Chem.*, **13**, 431 (1960).

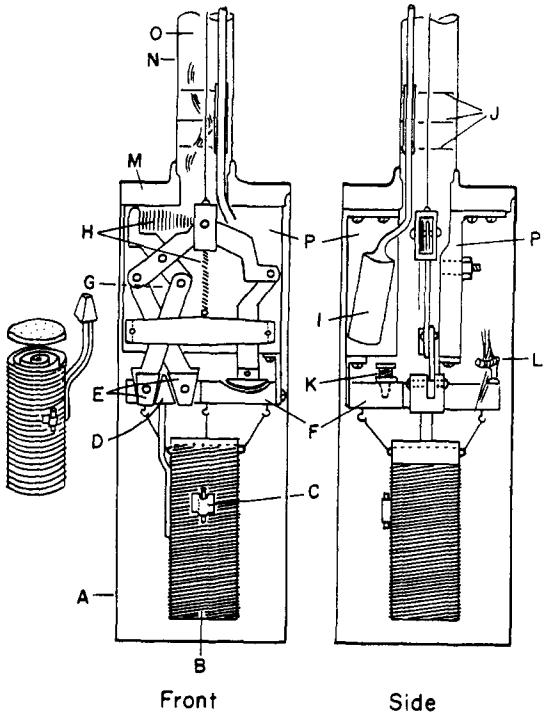

Fig. 2.—Close-up of helium-range calorimeter, block, thermal switch and accessory apparatus.

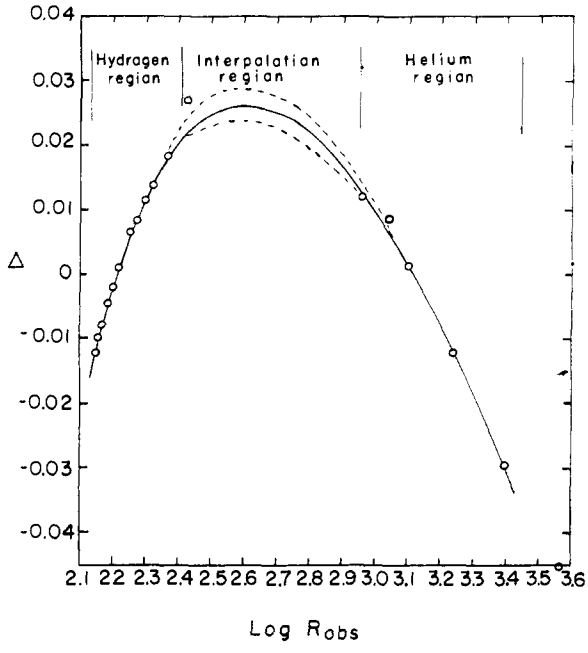

Fig. 3.—A typical Δ plot for thermometer calibration.

(N). Through it passed the electrical leads, which were led out of the apparatus by a Fusite high-vacuum seal (G), the vapor-pressure bulb line (O) and the wire that actuated the thermal switch. The tube also made possible evacuation of the calorimeter space by means of an oil-diffusion pump through the connection (H), also an O-ring seal. The flange (E) also contained the transfer port (I) for the refrigerant in the inner dewar and the connection (J) to the combination vent and safety valve (K). A Kovar seal (L) in the flange permitted electrical leads from the bath regulator (M) to be brought to the outside. Mounted at the top of the tube was the knob and traveling bolt (P) which raised and lowered the actuating wire for the thermal switch. The inner dewar was connected to a high-speed Kinney pump at (Q) (in back of the apparatus).

Figure 2 gives sectional views of the calorimeter and thermal switch. The copper can (A) was sealed to the copper disk (M) at the bottom of the tube (N) with Wood's metal. The calorimeter itself (B) was a copper cylinder (wall thickness 0.13 mm.) with a detachable top and a spiral copper inner vane to provide heat transfer from the calorimeter wall to the sample. The calorimeter is shown in perspective at the left of Fig. 3. The calorimeter was suspended from the copper block (F) by three strands of cotton thread. The thermal switch (G) was a series of levers terminating in two copper jaws (E) that were designed to grip the copper bit (D) which was part of the calorimeter. The jaws closed when the wire (O) was raised by the knob and bolt at the top of the tube. When the tension on the wire was released, two springs in the thermal switch (H) forced the jaws to open and release the bit of the calorimeter.

The block (F) was slotted to allow the thermal switch to operate. The block was suspended from the copper frames (P) supporting the thermal switch by stainless steel hangers. The block contained a block regulator (K) and a copper rail (L) to which the electrical leads from the calorimeter were glued. These leads were connected to the thermometer, a 56-ohm, 1/2-w, Allen–Bradley radio resistor (C), and to the calorimeter heater (represented as slanted lines on the calorimeter). The heater was 10 ft. of 0.00175 in. diameter manganin wire wrapped non-inductively around the upper and lower wall of the calorimeter.

The vapor-pressure bulb (I) was soldered to one of the frames. It was connected to a stainless steel tube which led to a manometer system. Three brass discs (J) served as a radiation trap but allowed penetration by electrical leads thermal switch wire and the line to the vapor-pressure bulb. To promote thermal equilibrium between the thermal-switch jaws and the surrounding bath, braids of copper wire (not shown) were soldered to the jaws and to the frames holding the mechanism. The frames were, of course, in good thermal contact with the bath, since they were bolted to the copper disc supporting the can.

The bath regulator (M) in Fig. 1 was held in place at the top of the can by cotton thread. Like the block regulator (K), it consisted of 2000 ohms of manganin wire wrapped around a spool, and a 10-ohm carbon radio resistor. The resistor was part of a resistance bridge, and the regulatory circuit was designed to provide a heating current to the manganin wire which was proportional to the imbalance of the resistor.

Appropriate electrical circuits were provided for energy input to the calorimeter, thermometry and regulation of bath and block temperatures; these have been fully described elsewhere.[11]

Temperature Scale 2–27°K.—For each series, the carbon-resistor thermometer was calibrated against the vapor pressure of liquid and solid hydrogen and liquid helium. The vapor-pressure bulb inside the can was connected by means of a stainless-steel capillary tube to a manometer system. Calibration was begun after the calorimeter had been cooled to some temperature in the hydrogen or helium region. The pressure inside the bulb was recorded by reading the differential height of the mercury manometer through a Gaertner cathetometer. Pressures below 60 mm. were observed on a second manometer filled with Octoil as a low-density (sp. gr. 0.98) manometer fluid. When both the vapor pressure and thermometer potential were steady, the readings were recorded. The thermometer measuring current was observed as well as the thermal e.m.f. in the thermometer circuit and manometer temperature. In each calibration, 10 to 14 separate points were taken in the hydrogen region and 6 to 8 points with liquid helium below 4.2°K.

The corrected manometer observations were converted to the absolute temperature in °K. by interpolation from the 1958 He^4 temperature scale[12] for the helium observations and by use of the vapor-pressure–temperature data of Brickwedde, Woolley and Scott[13] for the measurements on

(11) W. H. Orttung, Ph.D. Dissertation, University of California, 1961; also available as Lawrence Radiation Laboratory Report UCRL-9388, February 1, 1961.

(12) The 1958 He^4 Scale of Temperatures, *Natl. Bur. Standards Monograph 10*, part 2 (1960).

liquid and solid paralhydrogen. The absolute temperatures were estimated to be accurate to ±0.05% (~ 2 millideg.) in the helium region and about ±0.02% in the hydrogen region (2 to 4 millideg.).

Several semi-empirical equations have been suggested and used by other workers to relate the resistance and absolute temperature of a carbon-composition thermometer in this temperature region. In general these equations (*e.g.*, those of Clement and Quinnel[14]) involve the logarithm of the resistance and some function of the inverse temperature. In this research, the calibration data were approximately represented by a simple function

$$\log R = A + \frac{B}{T} + \frac{C}{T^2} \qquad (1)$$

where A, B and C are empirical constants determined for each calibration. Although the equations did not reproduce the data exactly, they served admirably as difference functions. For each calibration, such an empirical function was used to calculate

$$\Delta = (\log R_{\text{obsd.}})_T - (\log R_{\text{calcd.}})_T \qquad (2)$$

The Δ's were plotted as a function of log $R_{obsd.}$ and were found to define smooth curves in the regions 10 to 20°K. and 2 to 4.2°K. The region between 10 and 4.2°K., inaccessible to calibration, was spanned by a smooth curve through the observed Δ's. Figure 3 is a typical Δ plot. The dotted lines in the interpolation region show the estimated range of probable curves. The lowest temperature point in the hydrogen region appears to favor the upper dotted curve, but this point is given little weight because the attainment of thermal equilibrium through the solid hydrogen is slow and because there is a large uncertainty in the relationship of the very low vapor pressure to the actual temperature of the thermometer. The solid line in this region represents the probable curve. The indicated uncertainty in Δ is ±0.002 at a value of log $R_{obsd.}$ corresponding to 7.25°K. This uncertainty of ±0.002 in Δ means an uncertainty of ±0.025° in the absolute temperature, or ±0.35%. To calculate the temperature for any value of log $R_{obsd.}$ the corresponding value of Δ was read from the graph and used to find log $R_{calcd.}$. Then the quadratic equation 1 was solved for the positive root to give the temperature T.

With all factors considered, we estimate the maximum uncertainty of a *single* temperature observation in the interpolation region to be ±1%. Since, however, it is unlikely that a singularity in the temperature-resistance curve exists in this region, the uncertainty in two closely spaced observations of thermometer resistance to give $T_2 - T_1 = \Delta T$ for a heat-capacity measurement should be nearly the same and in the same direction. Thus the uncertainty of a heat-capacity measurement in this region should not exceed ±2%, although it is not possible to set a rigorous upper limit.

Heat Capacity Measurements, 2–27°K.—The energy input is computed from the heating current measured midway through the interval, the heater resistance and the time of heating. The temperature interval is calculated by conversion of the initial and final thermometer resistances to temperature values. The linear foredrift and afterdrift of the thermometer resistance were extrapolated to the midpoint of the heating period. The increment in temperature was increased gradually from 2 to 6% of the absolute temperature as the measurements proceeded from 2.5°K to above the normal boiling point of hydrogen. These small increments reduced to a negligible quantity the error involved in assuming a linear heat capacity between initial and final temperature.

The heat capacity of the empty calorimeter at T_{AV} was subtracted from the total heat capacity. One defined calorie was taken to equal 4.1840 joules. The sample weights were: (a) finely-divided, annealed Ag_2O, 40.851 g. or 0.1751 moles; (b) macrocrystalline Ag_2O, 71.570 g. or 0.3092 moles.

Heat Capacity Results

The Heat Capacity of Small-particle Annealed Ag_2O from 15 to 80°K.—The heat capacity of the empty gold calorimeter was measured and found to be the same as previously determined by Gerkin and Pitzer.[3] Then six series of measurements were made with the same sample of annealed Ag_2O in the calorimeter. The experimental results are given in Table II. Runs 1 and 2 covered the interval from 15 to 80°K.; Runs 4 and 6 were designed to examine the anomalous region more closely and extended only to about 40°K.; and Runs 3 and 5 were intended to investigate thermal hysteresis in the anomalous region.

TABLE II

HEAT CAPACITY OF SMALL PARTICLE ANNEALED Ag_2O

Units: cal./degree mole

T_{AV}, °K.	$C_{P_{Ag_2O}}$	T_{AV}, °K.	$C_{P_{Ag_2O}}$
Series 1		Series 3	
15.11	2.593	22.802	4.192
17.12	2.868	24.103	4.908
19.45	3.750	24.668	4.730
21.945	4.844	25.155	4.959
24.415	6.005	25.718	5.228
27.510	5.945	26.826	5.492
31.113	6.485	28.452	5.976
35.288	6.690	30.615	6.390
39.994	7.376	32.856	6.387
45.112	7.890	39.738	7.307
51.024	8.631	44.862	7.970
57.459	8.814	50.337	8.365
64.706	9.300	Series 4	
72.449	9.585	14.80	2.655
80.986	10.118	16.50	2.820
Series 2		18.43	3.284
14.25	2.135	20.469	4.197
16.09	2.573	22.447	5.081
17.84	3.161	24.273	5.688
19.63	3.761	25.851	5.810
21.371	4.574	27.328	5.752
23.071	5.383	29.030	6.066
24.591	5.826	31.053	6.683
26.068	5.710	33.441	6.414
27.687	5.899	36.167	6.988
29.446	6.228	39.454	7.732
31.457	6.412	Series 5	
33.722	7.181	14.66	2.706
36.323	7.001	16.39	3.128
39.464	7.074	18.54	3.366
43.207	7.663	20.669	4.253
47.412	8.003	22.761	5.228
51.882	8.436	25.679	5.737
56.866	8.802	29.054	6.376
61.568	9.102	32.494	6.436
66.720	9.402	36.230	7.638
71.961	9.642	40.458	7.372
77.434	9.782	44.992	7.861
82.985	10.069	49.705	8.269
		Series 6	
		27.990	5.754
		30.717	6.237
		33.410	6.408
		36.548	6.634
		39.958	7.223

The results are shown in Fig. 4 and clearly indicate a region of high heat capacity from 20 to 30°K.

(13) H. W. Woolley, R. B. Scott and F. G. Brickwedde, *J. Research Natl. Bur. Standards*, **41**, 379 (1948).

(14) J. R. Clement and E. H. Quinnel, *Rev. Sci. Instr.*, **23**, 216 (1952).

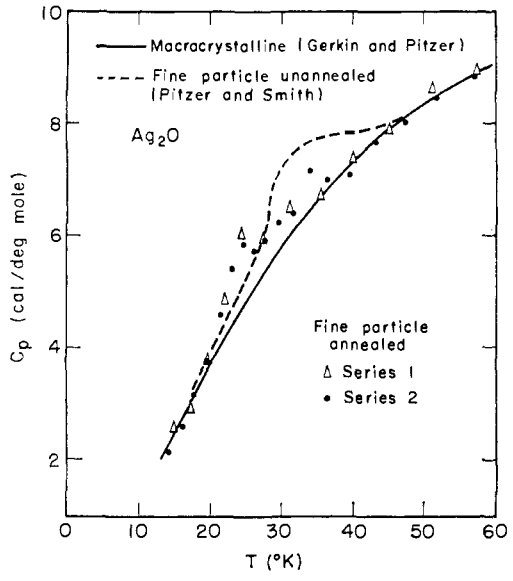

Fig. 4.—Heat capacity of annealed, finely-divided silver oxide. The series are designated 1 by Δ, 2 by O.

The data also reveal an unusually large scattering of points from any conceivable smooth curve between 30 and 40°K. The uncertainty of this type of heat-capacity measurement is usually estimated to be no more than ±1% above 20°K. and no more than ±5% below 20°K. The calculations were carefully rechecked for all points in this region. In each series, one or two points lie much further away from a smooth curve than the uncertainty in the measurements would appear to allow, and in all cases there are points from other series at that temperature that do fall near the smooth curve. Furthermore, the scattered points are all higher than the smooth curve; random errors would tend to distribute them below as well as above the base line.

Aside from the puzzling behavior between 30 and 40°K., the heat-capacity data are consistent with each other for the several series, and there is no indication that any significant change in the anomalous heat capacity from 20 to 30°K. occurs with repeated warming and cooling of a given sample.

The Heat Capacity of Ag_2O from 2 to 27°K.—Both the annealed small-particle sample of Ag_2O used in the previous measurements and macrocrystalline Ag_2O were investigated below 15°K.

Annealed small particle Ag_2O was measured in a double run, Series A,B. The first part consisted of cooling the sample to 9.5°K., followed by heat-capacity observations to 25°K. Then the calorimeter was cooled to 2.3°K. and the heat capacity measured up to 27°K. The results are given in Table III. The purpose of the split run was to observe the effect of initial temperature on the extent of the anomaly. The decreasing sensitivity of the thermometer above 25°K. precluded observations much above this temperature, and the runs were terminated shortly above 25°K. Figure 5 shows C; for both sections of the split run; the slight difference between these experimental results and the data reported from the other calorimeter

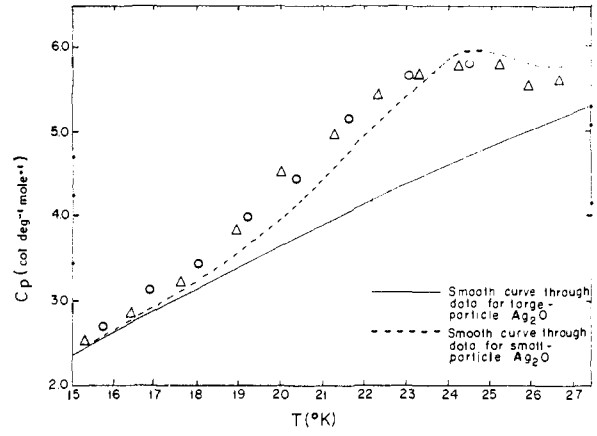

Fig. 5.—Comparison of the heat-capacity data for small-particle, annealed silver oxide obtained in the two different calorimeters. Δ indicates sample cooled to 10°K.; O, indicates sample cooled to 2.2°K.

(dotted line) is probably due to the different temperature scales.

TABLE III

HEAT CAPACITY OF SMALL-PARTICLE ANNEALED Ag_2O

Units: cal./degree mole

T, °K.	$C_{P_{Ag_2O}}$	T, °K.	$C_{P_{Ag_2O}}$
Series A		3.102	.1200
10.184	1.118	3.290	.1401
10.389	1.171	3.487	.1639
10.714	1.254	3.704	.1783
11.178	1.356	3.963	.2074
11.723	1.501	4.239	.2485
12.391	1.638	4.806	.3168
13.096	1.851	5.139	.3669
13.869	2.056	5.464	.4133
14.388	2.196	5.988	.4997
15.356	2.493	6.356	.5206
16.421	2.816	6.771	.6208
17.607	3.196	7.247	.6524
18.958	3.814	7.758	.7599
20.010	4.512	8.340	.8790
21.329	4.947	8.982	.9806
22.352	5.445	9.713	1.140
23.302	5.647	10.622	1.314
24.289	5.738	11.438	1.495
25.243	5.746	13.010	1.843
25.894	5.491	13.808	2.110
26.667	5.572	14.749	2.350
Series B		15.774	2.686
2.179	0.0418	16.875	3.089
2.223	.0518	18.090	3.343
2.285	.0628	19.203	3.977
2.396	.0680	20.361	4.466
2.543	.0775	21.653	5.149
2.712	.0880	23.084	5.666
2.907	.1036	24.567	5.801

The heat capacity of macrocrystalline Ag_2O was also measured from 3.2 to 23°K. in one continuous experiment. The results are given in Table IV. The data agree with the measurements of Gerkin and Pitzer on the same sample between 13 and 23°K. There is no localized anomaly.

Figure 6 illustrates the heat-capacity data for both samples of Ag_2O up to 25°K. The heat-

TABLE IV

HEAT CAPACITY OF MACROCRYSTALLINE Ag_2O
Units: cal./degree mole

T, °K.	$C_{P_{Ag_2O}}$	T, °K.	$C_{P_{Ag_2O}}$
3.328	0.2929	7.191	0.8807
3.358	.3479	7.679	0.9594
3.402	.2940	8.183	1.023
3.461	.3089	8.724	1.132
3.536	.3137	9.268	1.208
3.635	.3327	9.784	1.304
3.761	.3519	10.329	1.398
3.904	.3706	10.877	1.479
4.079	.3826	11.440	1.625
4.185	.4025	12.042	1.725
4.478	.4457	12.739	1.856
4.713	.4802	13.544	2.050
4.992	.5281	14.468	2.284
5.272	.5733	15.449	2.443
5.574	.6177	18.487	3.269
5.924	.6757	19.426	3.540
6.317	.7380	20.312	3.697
6.740	.8087		

capacity curves cross at 14°K, and below this temperature, the finely-divided annealed sample has a lower heat capacity than macrocrystalline Ag_2O.

The uncertainty in the heat capacity is estimated at ±1% in the regions where the thermometer was directly calibrated. In the interpolation region, the uncertainty from the temperature scale is approximately ±2%, but the individual points fit a smooth curve much better than this. The attainment of thermal equilibrium, as determined by the linearity of the temperature drift of the thermometer, was achieved in a few minutes after energy input at very low temperatures (2 to 4°K.) and high temperatures (18 to 27°K.); in the intermediate range, the time required increased to a maximum of 15 to 20 min. at about 10°K. and then decreased. Although the heat-exchange rate between the calorimeter and its surroundings was very low, there remained some uncertainty in the final heat capacity because of the rather long equilibrium time.

Thermodynamic Properties of Ag_2O

The thermodynamic functions of S^0 and $H_T^0 - H_0^0$ for Ag_2O were obtained by graphical integration of the curves C_P/T *vs.* T and C_P *vs.* T, respectively. This was done for both samples investigated. Table V gives these entropies as well as the value obtained by Debye function extrapolation by Pitzer and Smith for unannealed Ag_2O. The thermodynamic functions S^0, $(H^0 - H_0^0)$, and $(H_0^0 - F^0)/T$ at 298.15°K. for the three kinds of Ag_2O are given in Table VI. The functions for macrocrystalline Ag_2O were determined by combining the data of Gerkin and Pitzer above 15°K. with the data observed here below 15°K. For annealed small-particle Ag_2O, the heat-capacity data above 40°K. agree quite well with the results for the macrocrystalline sample, indicating that annealing has eliminated the extra heat capacity noted for unannealed Ag_2O. Although there are no data above 85°K. for the annealed, small-particle material, it seems reasonable to assume

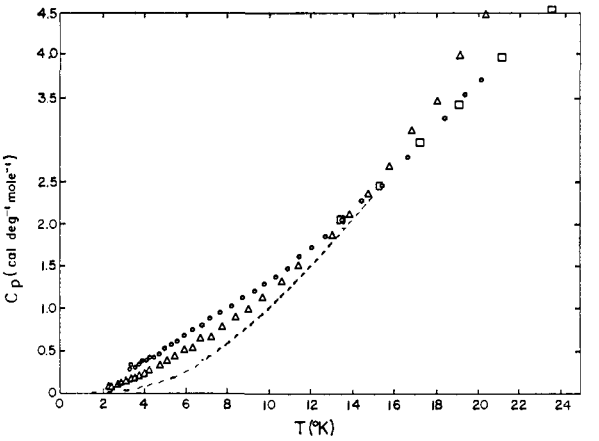

Fig. 6.—Heat capacity of silver oxide at lower temperatures. Macrocrystalline sample, this research ○, measurements of Gerkin and Pitzer □; small-particle annealed sample Δ. The dotted line is a Debye curve.

that the heat capacities of large and small particle annealed Ag_2O are practically the same up to 298°K. Finally, the previously published functions for unannealed Ag_2O are given.

TABLE V

ENTROPY OF Ag_2O

Type of Ag_2O	T (°K.)	S^0 (cal. deg.$^{-1}$ mole^{-1})	Source
Macrocrystalline	0–15	1.59 ± 0.02	This research
	15–298	27.32 ± .05	Ref. 3
	Total	28.91 ± .07	
Annealed, small-particle	0–15	1.32 ± .02	This research
	Anomaly	0.36 ± .02	This research
	15–298	27.32 ± .05	Based on ref. 3
	Total	29.00 ± .1	
Unannealed, small-particle	0–15	~0.97 ± .05	
	Anomaly	0.48 ± .03	
	15–298	27.64 ± .1	
	Total	29.09 ± .2	Ref. 4

TABLE VI

ENTROPY, ENTHALPY, AND FREE-ENERGY FUNCTIONS OF Ag_2O (ANNEALED) AT 298.15°K.

Sample	S^0 (cal./deg. mole)	$H^0 - H_0^0$ (cal./deg.)	$(H_0^0 - F^0)/T$ (cal./deg. mole)
Large particle (this research)	28.91 ± 0.07	3398 ± 5	17.55 ± 0.1
Small particle (this research)	29.00 ± .1	3397 ± 10	17.61 ± .1
Unannealed[a]	29.09 ± .2	3427 ± 5	17.60 ± .2

[a] Pitzer and Smith.[4]

It is interesting to note that the thermodynamic properties of large and small particle annealed Ag_2O at 298.15°K. are not very different, despite the presence of a heat capacity anomaly in small-particle annealed Ag_2O. The anomalous heat capacity found in this type of sample is almost exactly counterbalanced by the higher heat capacity of large-particle annealed Ag_2O below 14°K. This somewhat unusual behavior leads to the supposition that the diverse heat capacities of the various samples of Ag_2O all stem from the same underlying cause; that is, the somewhat bewildering variety of behavior with respect to

particle size, heat treatment, etc., might be interpretable in terms of the rather unusual crystal structure of Ag_2O.

Discussion

Silver oxide, which has the cuprite crystal structure, has an unusual feature that is almost certainly related in some way to the thermal anomalies. This structure has cubic symmetry[15] and involves fourfold, tetrahedral coördination at the oxygen atoms and linear, twofold coordination at silver atoms. Such low coördination numbers lead to a very open structure and in the cuprite structure one whole lattice is accommodated within the vacant space of a second and equivalent lattice. Thus half of the atoms of the crystal are connected by chemical bonds to one another, but there is no connection through bonds to any of the other half of the atoms. The second group of atoms are connected by bonds to form a second lattice which occupies the cavities in the first.

The absence of any chemical bond between the two ideal lattices implies only weak attractive forces between the two lattices. In Ag_2O the cavities are large enough that one does not expect appreciable repulsive forces so long as the two lattices remain in their ideal positions. But repulsive forces will arise if there is substantial movement of the atoms of one lattice away from their ideal locations in the middle of cavities in the other lattice.

Another feature of the silver oxide structure which may be important is the anisotropy of force field at the silver atoms which, because of their mass, will dominate the heat capacity at low temperatures. The linear O–Ag–O relationship indicates that the restoring force for Ag vibration transverse to the O–O axis will be much weaker than that along the O–O axis because the former is resisted only by bond angle bending forces while the latter involves bond stretching forces. This anisotropy of forces resembles somewhat the situation in the layer lattices, such as graphite, or in crystals of polymer molecules. Such crystals are known to depart from the T^3 heat capacity law at much lower temperatures than crystals with isotropic force fields.[16] Of course, in silver oxide the cubic symmetry of the total structure yields isotropic macroscopic force constants and the anisotropy is very local, while in graphite the anisotropy is macroscopic as well as microscopic. Full understanding of these effects must await a detailed analysis of the silver oxide vibration spectrum, but these factors presumably are related to the early departure of the Ag_2O heat capacity from the T^3 law shown in Fig. 6.

Special interatomic force situations arise at the surface of a crystal or at any internal defect. It seems likely that such forces at the surface and at defects will tend to displace the two interpenetrating lattices from their ideal relative position. The new unsymmetrical position will be one where the repulsive interlattice forces throughout the volume of the crystal balance the forces from surface atoms or interior defects. Let us now consider the effect of thermal energy in this hypothetical situation. The additional interlattice repulsive forces will raise the frequencies of many vibrational modes above the corresponding values for the ideal structure. At temperatures high enough to thermally excite these modes of vibration the ideal lattice will have a higher entropy than the distorted lattice. Thus there will be some temperature at which free energies of the ideal and distorted structures are equal and we may expect abnormal heat absorption associated with the structure change. Without more detailed analysis it is not feasible to say how sudden this transition will be, but there are cooperative factors which would contribute to sharpness.

This hypothesis is consistent with the effect of crystal size and perfection. Let us consider just the surface effect and assume that the energy favoring distortion is given by the product of the surface area A and a constant η. The entropy difference between ideal and distorted structures is δS. The transition temperature is just the ratio of these quantities

$$T_t = \frac{A\eta}{\delta S}$$

Since the entropy term will rise somewhat with temperature in the region of interest, we may expect T_t to increase with A but at a rate less than a direct proportionality. Table VII gives the relevant data; it is assumed that the surface area of sample c of Table I is the same as that of the similarly prepared calorimetric sample of Pitzer and Smith.

TABLE VII

ANOMALOUS ENTROPY AND RELATED DATA FOR Ag_2O

Sample	δS (cal./deg.)	T_t	A (m.²/g.)	η
Ppt., dried	0.55[a]	30	1.25	13
Annealed	0.44	23	0.60	17
Macrocrystalline	(0.3)	(6)	0.07	25

[a] Recalculated from the data of Pitzer and Smith and the base curve from Gerkin and Pitzer.

This research was carried out under the auspices of the U.S. Atomic Energy Commission.

(15) R. W. G. Wyckoff, *Am. J. Sci.*, **3**, 184 (1922).

(16) P. H. Keeson and N. Pearlman, *Phys. Rev.*, **99**, 1119 (1955).